





OPTIMISATION OF A NACELLE ELECTRO-THERMAL ICE PROTECTION SYSTEM FOR ICING WIND TUNNEL TESTING

Mariachiara Gallia^{1*}, Alessandro Carnemolla², Marco Premazzi², Alberto Guardone¹

¹ Department of Aerospace Science and Technology, Politecnico di Milano, Via La Masa, 34, 20156 Milano, Italy

² Leonardo S.p.a., Piazza Monte Grappa, 4, 00195 Rome, Italy

Abstract

Aircraft are equipped with ice protection systems (IPS), to avoid, delay or remove ice accretion. Two widely used technologies are the thermo-pneumatic IPS and the electro-thermal IPS (ETIPS). Thermo-pneumatic IPS requires air extraction from the engine negatively affecting its performances. Moreover, in the context of green aviation, aircraft manufacturers are moving towards hybrid or fully electric aircraft requiring all electric on-board systems. In this work, an ETIPS has been designed and optimised to replace the nacelle pneumatic-thermal system. The aim is to minimise the power consumption while assuring limited or null ice formation and that the surface temperature remains between acceptable bounds to avoid material degradation. The design parameters were the length and heat flux of each heater. Runback ice formations and surface temperature were assessed by means of the in-house developed PoliMIce framework. The optimisation was performed using a genetic algorithm, and the constraints were handled through a linear penalty method. The optimal configuration required 33% less power with respect to the previously installed thermo-pneumatic IPS. Furthermore, engine performance is not affected in the case of the ETIPS. This energy saving resulted in an estimated reduction of specific fuel consumption of 3%, when operating the IPS in anti-icing mode.

Keywords: in-flight icing; ice protection systems; optimisation; genetic algorithms; nacelle

Type of the work: research article

1. INTRODUCTION

In-flight ice accretion occurs when an aircraft is flying through a cloud of supercooled water droplets. These droplets are in a meta-stable equilibrium state because their temperature is below the freezing point, but they are still liquid. Once these droplets impact on a moving surface, this equilibrium is broken. Droplets can freeze instantaneously or retain their liquid phase and move on the surface, forming a thin liquid film, or a combination of both, depending on the heat fluxes involved.

Ice accretion on aircraft surfaces has a significant effect on aircraft performance, and every year, several accidents are caused by in-flight icing [1,2]. Ice can form on the most exposed zones such as wing leading edges, engine intakes, pitot tubes, propellers and vents. These formations can lead to performance degradation like lift reduction and drag increase. Wind tunnel tests have shown that ice accumulations no thicker than a piece of coarse sandpaper can reduce lift by 30% and increase drag by 40% [2]. Larger

accretions can increase drag by 80% or even more. Moreover, ice formations on the aircraft can lead to stall at much lower angles of attack and can increase the weight, leading to a reduction of aircraft stability. Furthermore, ice can lead to failures of the engine and of measurement tools. Engine failure can be caused either by blocking or damaging compressor blades, icing the carburetor or by ice crystal injection [3]. These events can interfere with air operations and require unscheduled maintenance.

Manufacturers must be able to certificate that the aircraft is able to operate under icing conditions. Aircraft are commonly equipped with ice protection systems (IPS) to prevent, delay or reduce ice accretion on critical parts. IPS can operate in two modes: anti-icing and de-icing. In the former, ice accretion is prevented, while in the latter, ice formations are removed once the system is actuated. A widely used technology in commercial, defence and business aircraft is the pneumatic-thermal protection. The air is supplied to the air cycle machines and exhausted through the piccolo tube of the IPS to heat the surfaces at risk of ice accretion. This system can be very inefficient because the temperature of the air bled from the engine must be down-regulated for safety reasons before being used by the IPS, and the extraction of hot air from the engine can negatively affect engine performances. Another widely used technology is the electro-thermal IPS (ETIPS) that exploit the Joule effect, which occurs when current goes through a resistive component, to heat the surface. Several heater pads are embedded in the inner substratum; these can be activated continuously to prevent ice formation, anti-icing mode, or actuated to remove an already formed ice layer, de-icing mode. The ETIPS is the preferred method for rotor blades and probes since it is adaptable to complex surfaces and its weight is restrained. Moreover, with aircraft manufacturers moving towards hybrid or fully electrical aircraft, this technology is becoming more widely adopted even for aircraft's wings and nacelle.

The design and certification process of these IPS generally includes wind tunnel or flight tests. Two main problems arise: the high cost of these tests and the availability of suitable facilities. Due to this in the past years, there has been a large research effort on the development of numerical models that could help in the preliminary design of IPS and to improve the understanding of the physics. Some examples of numerical codes include ANTICE [4], FENSAP-ICE [5], PoliMIce [6], the work by da Silva et al. [7,8] and the work by Bu et al. [9]. Thanks to these developments recently, there has been some research effort to optimise IPS power consumption. In the work by Pourbagian and Habashi [10], the geometric parameters of an ETIPS of a wing have been optimised by means of multi-adaptive direct search. Furthermore, in another work by Pourbagian et al. [11], an anti-ice ETIPS for a wing was optimised considering various different constraints like maximum ice growth, minimum surface temperature and liquid film height at the end of the protected region. Pellisier [12] optimised a pneumatic IPS for a wing by minimising the power consumption while ensuring that all the water was evaporated.

In this work, an ETIPS for a nacelle test article for icing wind tunnel (IWT) testing has been designed and optimised to replace a previously used thermo-pneumatic IPS in order to reduce the power consumption. The optimisation was performed by means of a genetic algorithm because it is able to deal with complex problems like nonlinear functions and multiple local minima as in this case. Four different constraints were investigated considering a maximum admissible ice formation and surface temperature bounds. In Section 2, the numerical framework, the baseline design of the ETIPS and the optimisation procedure are presented. The results obtained from the optimisation are shown and discussed in Section 3. Lastly, in Section 4, final remarks are presented.

2. METHODS

2.1. Numerical modelling

In order to optimise the power consumption of the ETIPS, it is necessary to evaluate the amount of ice accretion and the surface temperature to determine which designs are feasible and which are not.

These quantities are computed by solving energy and mass conservation equations in control volumes on the nacelle surface. To this purpose, different modules are required. Indeed, in an anti-ice simulation, it is first necessary to determine the flow field around the nacelle. This is done through the open-source software SU2 [13]; in this work, an Euler simulation is performed; boundary layer quantities like shear stress and convective heat transfer coefficient are computed through a boundary layer model based on the work by Silva et al. [14]. Once the flow field is known, the trajectory of cloud particles are evaluated by means of the Lagrangian particle tracking PoliDrop [15]. This allows us to compute the impinging water distribution on the airfoil surface, i.e. the collection efficiency β . The collection efficiency is defined as the ratio between the far-field area and the surface area enclosed by the same droplet trajectories. Finally, in the thermodynamic solver PoliMIce [16,17], conservation equations are solved to obtain the surface temperature and the amount of ice that forms on the nacelle surface. The anti-ice model implemented in PoliMIce [16] is based on the work by da Silva et al. [7,8]; the liquid film model is adapted to anti-ice from the work of Myers [18]. The model conservation equations are here reported for clarity. Further details can be found in the work by Gutiérrez et al. [16]. Two energy conservation laws are solved in PoliMIce: first in the substratum of the nacelle to consider heat conduction inside the heater mats of the IPS:

$$\frac{d}{ds} \left(k_{wall} H \frac{dT_{surf}}{ds} \right) - F h_{H_2O} (T_{surf} - T_{H_2O}) + \ddot{q}_{IPS} - (1-F) [h_{air} (T_{surf} - T_{rec})] = 0. \quad (1)$$

Conduction is only considered in the streamwise direction since the heating elements are thin and conduction in the normal direction can be neglected. The multilayered substratum is modelled as a unique layer with an equivalent thermal conductivity k_{wall} . It can be estimated by means of electrical analogy, considering the thermal resistance of the materials forming the heating element in parallel.

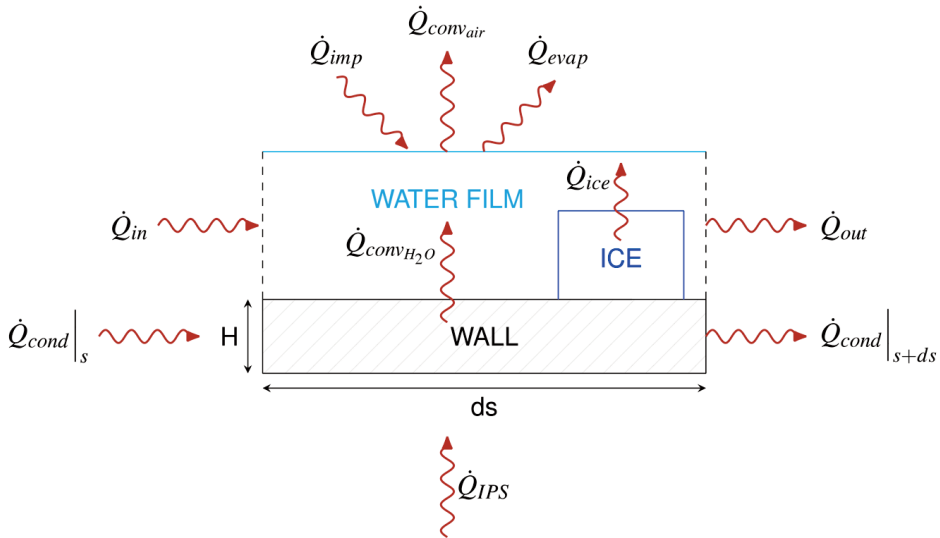


Figure 1. Contributions to energy conservation in a finite volume [16].

The other energy conservation equation is related to the water film and includes all heat flux contributions that are shown in Fig. 1; the complete equation reads as follows:

$$\begin{aligned}
& FAh_{air} (T_{rec} - T_{H_2O}) + FAh_{H_2O} (T_{surf} - T_{H_2O}) + m_{in} c_{\rho_{H_2O}} (T_{in} - T_{ref}) \\
& - \dot{m}_{out} c_{\rho_{H_2O}} (T_{out} - T_{ref}) + \dot{m}_{imp} \left[c_{\rho_{H_2O}} (T_{\infty} - T_{ref}) + \frac{V_{\infty}^2}{2} \right] \\
& - \dot{m}_{evap} \left[i_{l-v} + c_{\rho_{H_2O}} (T_{H_2O} - T_{ref}) \right] + \dot{m}_{ice} \left[i_{l-s} + c_{\rho_{H_2O}} (T_{H_2O} - T_{ref}) \right] = 0.
\end{aligned} \tag{2}$$

The unknowns of the two energy conservation equations are the water temperature T_{H_2O} and the surface temperature T_{surf} .

The runback water mass fluxes are determined through the liquid film model. The model is based on lubrication theory; the layer is considered to be thin so the liquid film velocity only depends on the height of the film. The mass conservation can therefore be written as follows:

$$\frac{\partial \delta_f \bar{u}_f (\delta_f, s)}{\partial s} = \frac{\dot{m}_{imp}'' - \dot{m}_{evap}'' - \dot{m}_{ice}''}{\rho_{H_2O}}. \tag{3}$$

Once the liquid film thickness and velocity are known, the runback water mass fluxes can be determined. The evaporative mass flux is evaluated by means of the heat and mass transfer analogy. While the freezing mass rate depends on the incoming mass of water and the water temperature, freezing is considered to occur in a range of 273.15 ± 0.05 K; if T_{H_2O} is below the lower bound, all water freezes; if it is above the upper bound, none of the water freezes; lastly, if the equilibrium temperature is within the freezing bounds, the freezing rate depends on the normalised difference between the temperature T_{H_2O} and the lower bound.

The solver takes as inputs the results from CFD (Computational Fluid Dynamics) and particle tracking. The stagnation point is then identified from numerical data as the point of minimum velocity. This is the point where the boundary layer computations determine the shear stress and the heat transfer coefficient for a fixed T_{surf} and T_{rec} . Then, the conservation laws in Eqs (1), (2) and (4) are solved for each control volume from the stagnation point till the leading edge. These equations are non-linear since h_{air} depends on T_{surf} and h_{H_2O} depends on T_{H_2O} . Eq. (1) can be rewritten to express T_{surf} as a function of T_{H_2O} . The only unknown is therefore T_{H_2O} , and the problem can be solved using the bisection method applied to Eq.(2). This is repeated in every control volume from the leading to trailing edge on both sides. The surface temperature distribution, the runback water mass fluxes, the rate of ice accretion and the water equilibrium temperature are obtained. T_{surf} and T_{rec} are updated, and boundary layer calculations are repeated. The loop is performed until the L_{∞} norm of the surface temperature difference between two subsequent iterations is below a given tolerance, that is, $\max |T_{surf, i}^{it} - T_{surf, i}^{it-1}| < \varepsilon$, where $\varepsilon = 10^{-2}$.

2.2. Electro-thermal IPS design

The nacelle test article for an IWT is designed starting from a business aircraft nacelle and then extruding this section for the entire height of the wind tunnel test chamber. Since the geometry does not present particular 3D features, the 2D section of the test article was used for the design and optimisation of the ETIPS to reduce the computational cost.

The ETIPS design comprises a set of four heaters that operate in anti-icing mode placed in the region close to the leading edge, which is the most exposed zone to ice accretion. A schematic representation of the design can be seen in Fig. 2.

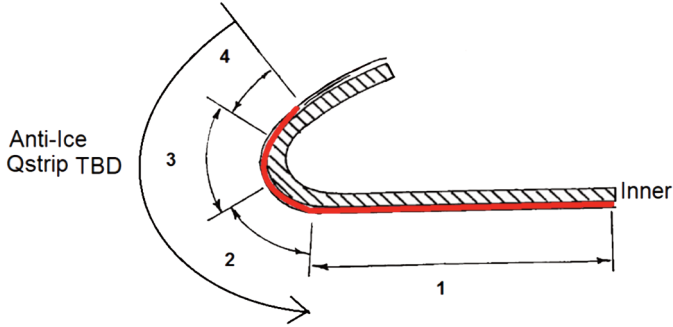


Figure 2. Schematic representation of the ETIPS of the nacelle. ETIPS, electro-thermal ice protection systems.

The lower part represents the inboard of the nacelle while the upper surface represents the outboard. The heated lip has a total non-dimensional length of $l_{heated} = 0.252$; the extension of this region has been designed according to impingement limits in CS-25 APPENDIX O conditions, i.e. super large droplets.

The composition of the multilayered heaters has been taken from the experimental work of Al-Khalil et al. [4]. The heater resistance is embedded inside a four-layer composite panel including erosion shield, elastomer, fibreglass and silicone foam. The material properties are presented in Table 1, and a schematic view of the multilayered heating element is shown in Fig. 3.

Table 1. Heating element layers with material properties [4].

Material	$k \left[\frac{W}{m K} \right]$	$\rho \left[\frac{Kg}{m^3} \right]$	$c_p \left[\frac{J}{Kg K} \right]$
Heating element (Alloy 90)	41.02	8,906.26	385.19
Erosion shield (SS 301 HH)	16.27	8,025.25	502.42
Elastomer (Cox 4300)	0.256	1,384	$1,256.04 \pm 125.6$
Fibreglass/epoxy composite	0.294	1,794.07	1,570.05
Silicone foam insulation	0.121	648.25	$1,130.44 \pm 125$

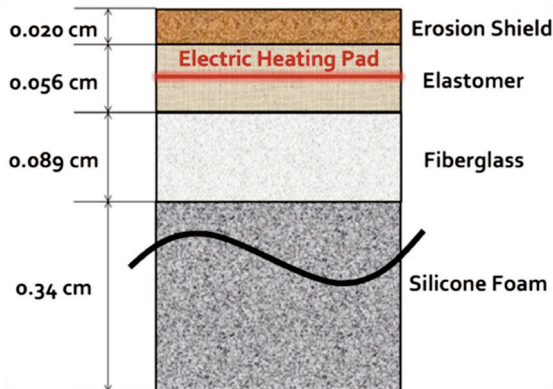


Figure 3. Schematic view of the heater layers [11].

According to certification specifications (CS) of the European Aviation Safety Agency (EASA) [19,20], several environmental and flight conditions must be tested in order to guarantee safety in different adverse conditions that an aircraft could encounter during flight. Regarding engines, when they are operating in the atmospheric icing condition specified in the CS, it must be guaranteed that they don't suffer deterioration of performances. Some of the situation listed in the CS are take-off, en-route and landing. Based on a previous experimental campaign, it has been chosen to design the IPS in the worst-case scenario, that is, the test condition at lower ambient temperature and longer exposure time. The IWT parameters used for the simulation for the design and optimisation of the IPS are presented in Table 2.

Table 2. IWT parameters used for the design of the IPS.

	IWT parameters
$\alpha [^\circ]$	1.70
$u_\infty \left[\frac{\text{m}}{\text{s}} \right]$	67.48
$T_\infty [\text{K}]$	259.95
$\rho \left[\frac{\text{kg}}{\text{m}^3} \right]$	1.2886
$p_\infty [\text{Pa}]$	101,325
$MVD [\mu\text{m}]$	28.0
$LWC \left[\frac{\text{g}}{\text{m}^3} \right]$	0.583
$\Delta t [\text{s}]$	594

IWT, icing wind tunnel.

2.3. Optimisation procedure

The aim of the optimisation was to reduce the overall energy consumption while assuring that there is no or limited ice formation and that the surface temperature remains between acceptable bounds to avoid material degradation. As presented in Sub-Section 2.2., the IPS is composed of four heaters that can be activated separately with different heat fluxes. The design vector x comprises the heat flux of each of the four heaters and the length of three heaters. The fourth heater length is fixed by the total length of the protected region. Four different constraints have been considered to determine the best trade-off between safety and power saving in a fixed operating condition. First, a very conservative constraint was considered, where designs with ice formation on the inboard of the nacelle were considered unfeasible. The second constraint was related to the protected region surface temperature, which was set between a minimum value of $T_{min} = 280.15$ K, to ensure a limited ice formation, and a maximum value of $T_{max} = 294.15$ K, to avoid material degradation. Then, these two constraints have been combined to impose a new one where the designs were considered to be unfeasible if there was ice formation or the temperature was above $T_{max} = 294.15$ K. Lastly, the constraint on the maximum surface temperature was not modified while the ice formation constraint was relaxed and limited ice formation was allowed. Following the CS [19,20] of EASA, it is admissible that forms on the inboard an ice build-up sheet or slab not to exceed a maximum local thickness of: $a \cdot b \cdot B$, where $a = 0.1270$ m, $b = 0.3048$ m and $B = 0.0095$ m. Considering a safety factor, the maximum acceptable ice height was set to $B_{max} = 0.00464$ m. The ice height B is evaluated from the rate of ice accretion \dot{m}_{ice} as follows:

$$B = \frac{\dot{m}_{ice} \Delta t l_{span}}{\rho_{ice} a b} \quad (4)$$

where Δt is the exposure time, while l_{span} is the span of the nacelle test article. The constraints were handled by a linear penalty method; the amount of constraint violation was integrated in the objective function as a penalty. The penalty was different for each constraint, and the formulation of each penalty is presented in Table 3.

Table 3. Penalty for each constraint.

Constraint	Description	Penalty ice	Penalty temp.
$\dot{m}_{ice}'' = 0$	No ice	$2.26 \cdot 10^7 \sqrt{\sum_{j=1}^N \dot{m}_{ice_{mb}}''(s_j)}$	-
$T \in [T_{min}, T_{max}]$	Temp.	-	$2.26 \cdot 10^7 \sqrt{\left 1 - \frac{T_{surf}(s_j)}{T_{min/max}} \right }$
$\dot{m}_{ice}'' = 0$ $T \leq T_{max}$	No ice & temp.	$4.52 \cdot 10^7 \sqrt{\sum_{j=1}^N \dot{m}_{ice_{mb}}''(s_j)}$	$1 \cdot 10^5 \sqrt{\sum_{j=r}^R \left 1 - \frac{T_{surf}(s_j)}{T_{max}} \right }$
$B \leq B_{max}$ $T \leq T_{max}$	Ice & temp.	$4.52 \cdot 10^7 \sqrt{\left \frac{\sum_{j=1}^N \dot{m}_{ice_{mb}}''(s_j) \Delta t l_{span}}{\rho_{ice} a b} - B_{max} \right }$	$1 \cdot 10^5 \sqrt{\sum_{j=r}^R \left 1 - \frac{T_{surf}(s_j)}{T_{max}} \right }$

Different proportionality factors are assigned to each constraint in order to obtain a penalty that was of the order of magnitude of the objective function. When two penalties are applied, a larger penalty factor is given to the constrain related to ice formation. The formulation of the optimisation problem can be written as follows:

$$\text{minimise}_{x \in \mathbb{R}^7} l_{span} \sum_{i=1}^4 \dot{q}_{IPS,i}'' \Delta l_i + \text{penalty} \quad (5)$$

$$\dot{q}_{IPS,i}'' \geq 2325 \frac{W}{m^2} \quad (6)$$

$$\dot{q}_{IPS,i}'' \leq 46500 \frac{W}{m^2} \quad (7)$$

$$\sum_{i=1}^4 \Delta l_i = l_{heated} \quad (8)$$

where l_{heated} is the total length of the heated surface as described in Sub-Section 2.2.

2.4. Genetic algorithms

Genetic algorithms (GAs) are randomised search algorithms; they are part of the evolutionary algorithms that are inspired by the natural process of evolution. A random initial population is initialised, from this the fittest individuals produce offspring that inherit parents' characteristics. Then, the offspring individuals are added to the next generation, and the process is repeated till convergence or the maximum number of generations is reached. GAs are capable of dealing with complex problems including nonlinear

objective functions and multiple local minima. Moreover, GAs are widely proven and versatile algorithms. Along with this, there are some disadvantages of GAs like the fitness function formulation and the population size, and other important parameters need to be carefully chosen, where setting those parameters in an improper way could lead to slow or no convergence [21]. The first step of GA (Genetic Algorithm) is the initialisation of a random population; in this work, the population size was set to 500 individuals following the work by Gutiérrez et al. [6]. Each individual is characterised by a chromosome containing the input parameters, known as genes and encoded as bits, and by a value of the objective function. Once the initial population has been initialized, the evolutionary process begins exploiting the genetic operators of selection, crossover, mutation and elitism. During selection, the fittest individuals are chosen through a roulette wheel selection process. The individuals with the lower fitness value have a higher probability to be chosen as parents. Then, a crossover point is randomly selected, and the genes of the parents are swapped till the crossover point. In the mutation stage, bits of the individuals are randomly changed to maintain the diversity in the population. Lastly, elitism is performed, that is, the individual with the best fitness is directly transferred to the next generation to avoid losing the best design. In this work, different GA operators have been tested: mutation-based GA (M-GA → Mutation-Genetic Algorithm), crossover-based GA (C-GA → Crossover-Genetic Algorithm) and a combination of them (CM-GA → Crossover Mutation-Genetic Algorithm). As suggested by Deb [22], the crossover probability was set equal to 0.9, while the mutation probability to $1/l$, where l represents the sum of all the genes; in this work, $l = 126$. Due to the non-deterministic nature of the GA for a fixed constraint and genetic operator, each run has been performed three times and was stopped after 400 generations.

3. RESULTS

The results of the optimisation are now presented for each type of constraint and compared with the performance of the thermal-pneumatic IPS. The total power consumption is evaluated by multiplying the heat flux of each heater by its length Δl_i ; then, four values are summed and multiplied for the entire test article span l_{span} , as stated in Eq. (9).

$$P = l_{span} \cdot \sum_{i=1}^4 \dot{q}_{IPS_i}'' \Delta l_i \quad (9)$$

Moreover, the mass of ice is evaluated starting from the rate of ice accretion by multiplying it for the entire span l_{span} and the total exposure duration, that is, $\Delta t = 594$ s.

Figure 4 presented the evolution of the fitness function of the best design over the number of generations for no ice constraint runs as example of convergence history. Table 4 presents for each constraint the parameters of the best designs: the power consumption per unit span, the mass of ice that forms in the inboard and in the outboard per unit span and the minimum and maximum surface temperature in the protected region. The last column presents the genetic operator for which the best design was obtained.

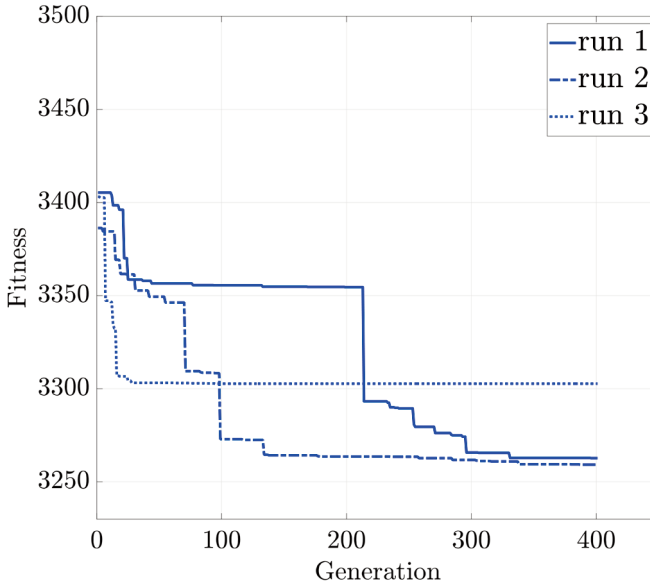


Figure 4. Convergence history over the number of generations for no ice constraint runs.

Table 4. Best design for each constraint.

Constraint	$\frac{P_{\min}}{l_{span}} [\text{W/m}]$	$\frac{m_{ice, inb}}{l_{span}} [\text{g/m}]$	$\frac{m_{ice, out}}{l_{span}} [\text{g/m}]$	$T_{\max} [\text{K}]$	$T_{\min} [\text{K}]$	GA
No ice	3305.65	0	320.77	326.11	266.75	CM-GA
Temp.	1657.74	328.29	306.50	287.57	280.18	C-GA
No ice & temp.	3452.95	0	316.59	325.05	275.74	M-GA
Ice & temp.	1517.02	323.72	319.57	294.14	273.21	CM-GA

It can be noticed that, as it was expected, the lowest power consumption was obtained for the constraints where ice is allowed to form on the surface. In both cases, the predicted mass of ice is below the value required by CS [20] $m_{ice}/l_{span} = 726.38 \text{ g/m}$. In all cases, there is ice formation on the outboard part of the nacelle, and all constraints have a similar value; this is reasonable since there was no constraint that impeded it. Moreover, in the design of the complete IPS, which is not shown here, it was introduced as an additional strip on the outboard that can work in de-icing mode to remove the formed layer of ice. Regarding the temperature values, it must be noted that in the case of the no ice and temperature constraint, the latter is violated. Indeed, the two constraint have opposite requirements: by decreasing the surface temperature, the ice formation is increased and vice versa. Since, as stated in Sub-Section 2.3, the ice constraint had a larger weight with respect to the temperature one which is violated when performing the optimisation. Furthermore, it can be noticed that there is an improvement in power consumption when the ice formation is limited through a constraint with respect to the limitations caused by the lower bound of the protected region surface temperature. Indeed, in the fourth constraint, the minimum value of the temperature is far below the lower temperature bound. This means that, if a minimum temperature constraint is applied, the value could be lowered to reduce the required power

consumption without exceeding the maximum ice formation allowed by CS [20]. Figure 5 shows a comparison of PoliMIce results for the best designs for each constrain presented in Table 4.

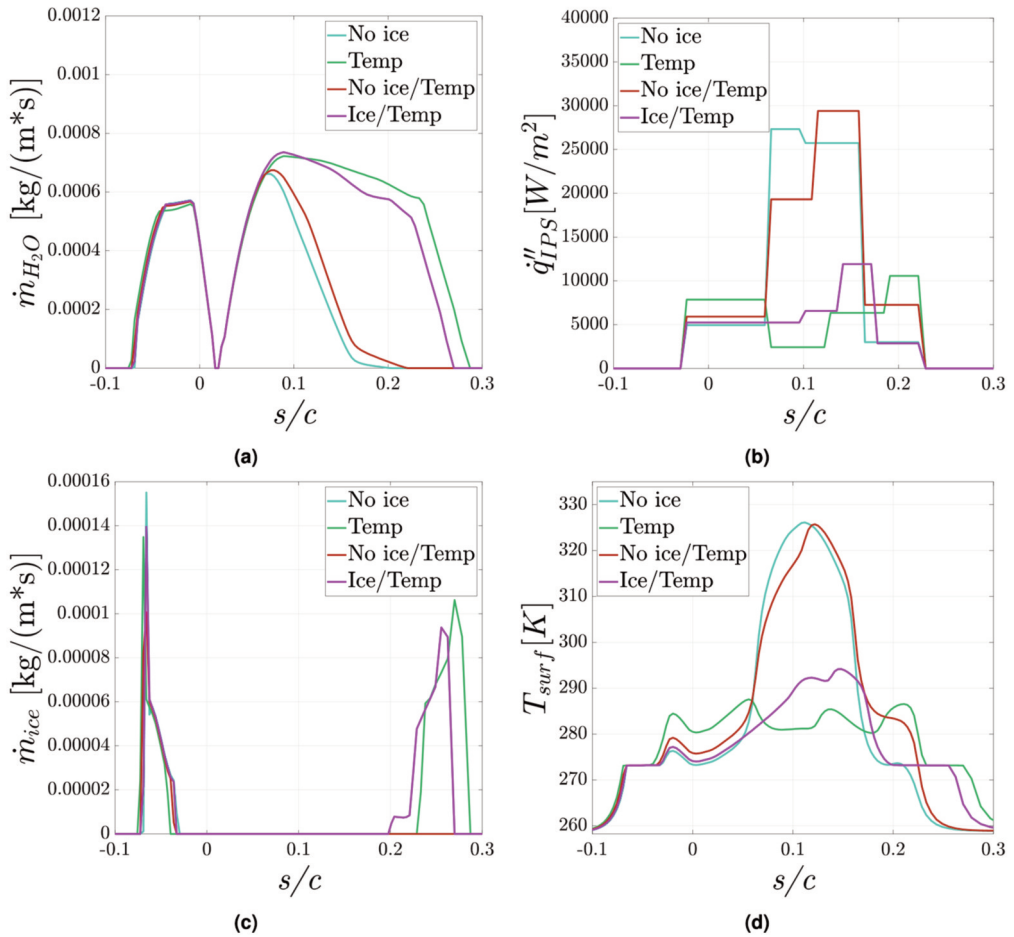


Figure 5. Result comparison for the best designs for each constraint. (a) runback water; (b) heat fluxes; (c) ice accretion rate; (d) surface temperature. $s/c < 0$ represents the outboard, $s/c > 0$ the inboard.

In all plots, the x axis represents the curvilinear abscissa normalised by the chord. $s/c = 0$ is the stagnation point; positive values ($s/c > 0$) refer to the inboard of the nacelle while negative values ($s/c < 0$) refer to the outboard. Figure 5b shows the heat flux distribution for each constraint; the protected region was imposed to be the same for all constraints, but the length of each heater may change from one to the other. Moreover, in the case of the two ‘no ice’ constraints, it can be noticed that there is a large heat flux peak after the stagnation point in the inboard so that all the water is evaporated before reaching the protected region limits.

This is not the case for the *Temp.* and *Ice & Temp.* constraints; in this case, the heat fluxes are constrained to remain low in order to limit the maximum temperature on the protected zone. This causes a lower evaporation rate and therefore a larger amount of runback water flowing past the protection limits, leading to ice formation in the inboard of the nacelle. Fig. 5a shows the runback water mass flux. The trend in the outboard is similar for all the constraints, while there is a large discrepancy in the inboard

among constraints that admit ice formation and those that don't. This trend is also visible in Figure 5c where the rate of ice accretion is very similar for all constraints in the outboard, while in the inboard, the rate of ice accretion is zero where it was constrained, $\dot{m}_{ice} = 0 \text{ kg}/((\text{m s}))$, as expected. While in the other constraints, there is water flowing past the protected region leading to runback ice formation in the inboard.

In the case of *Ice & Temp.* constraint a small amount of ice starts forming already in the protected region. Lastly, Figure 5d presents the surface temperature trend on the protected region; it is clear that the temperature is lower along the whole surface for the *Temp.* and *Ice & Temp.* Furthermore, two regions, one in the inboard and one in the outboard, can be singled out, where the temperature is approximately constant and equal to the freezing temperature. This is the region where ice formation occurs, and it is clear by comparing these regions with Figure 5c. Lastly, a comparison with the previously tested thermo-pneumatic system has been performed, as shown in Table 5.

Table 5. Power consumption comparison.

IPS (constraint)	Thermo-pneumatic	ETIPS (no ice)	ETIPS (temp)	ETIPS (no ice/temp)	ETIPS (ice/temp)
Lip surf. (m ²)	0.14	0.19	0.19	0.19	0.19
\dot{q}_{IPS}'' (kW/m ²)	10	13.02	6.53	13.60	5.97
\dot{q}_{IPS} (kW)	1.4	2.47	1.24	2.58	1.13

ETIPS, electro-thermal ice protection systems; IPS, ice protection systems.

Lip surface represents the protected region of the nacelle; the ETIPS covers a larger region, and this is due to the fact that it has been design to comply with APPENDIX O CS [19,20]. \dot{q}_{IPS}'' is the average specific power along the heaters, as it can be noticed this is lower in the case of the ETIPS in the case of the *Temp.* and *Ice & Temp.* The specific power outperforms the thermo-pneumatic system that also presented a limited ice formation both in the inboard and in the outboard. While in the safer conditions where ice formation in the inboard is not allowed, the required power becomes higher. Compared with the thermo-pneumatic pneumatic IPS, the electrothermal IPS for the *Ice & Temp.* constraints saves >30% energy. Moreover, the energy saving results in a reduction of 'specific fuel consumption' of 3%, when the IPS is activated. This consideration arises from a comparison of a thermo-pneumatic IPS and an ETIPS where each IPS provides the same thermal energy in order to heat the lip surface. Indeed, engine performances improve if only mechanical power and not pneumatic is extracted. Therefore, if a small amount of ice formation is accepted, the *Ice & Temp.* constraint presents lower power consumption with respect to the thermo-pneumatic IPS. Nevertheless, for a safer condition, the *No Ice & Temp.* constraint needs to be considered, and consequently, a higher power consumption is required.

4. CONCLUSION

In this work, an ETIPS for an engine nacelle for IWT testing has been designed and optimised to replace a previously tested thermo-pneumatic IPS. The design composed of four different heaters with variable lengths that could be activated with different heat fluxes. The optimisation was performed through a genetic algorithm; the aim was to minimise power consumption. Four different constraints have been considered for the design: No Ice, Temp., No Ice & Temp. and Ice & Temp. As expected, from the optimisation arose the lowest power consumption if some ice is allowed to form in the inboard as in constraint Ice & Temp. and Temp, whereas if a conservative design is considered, that is, no formation in the inboard of the nacelle, more power is required and the surface temperature has higher values.

Indeed, evaporating all the water before the end of the protected region requires larger heat fluxes that raise the surface temperature. Furthermore, it was found that, considering the *Ice & Temp.* constraint, the power required by the ETIPS is 33% lower with respect to the thermo-pneumatic system. This corresponds to lower fuel consumption and consequently less pollution, contributing to the development of greener and safer air transport.

Copyright statement: The authors confirm that they, and/or their company or organisation, hold copyright on all of the original material included in this paper. The authors also confirm that they have obtained permission from the copyright holder of any third-party material included in this paper, to publish it as part of their paper. The authors confirm that they give permission or have obtained permission from the copyright holder of this paper, for the publication and distribution of this paper as part of the AEC (Aerospace Europe Conference) proceedings or as individual off-prints from the proceedings.

References

- [1] Cole, J. and Sand, W. "Statistical Study of Aircraft Icing Accidents". *Proceedings 29th Aerospace Sciences Meeting*. p. 558. 1991. Reno, Nevada (USA).
- [2] Jones, S.M., Reveley, M.S., Evans, J.K., and Barrientos, F.A. "Subsonic Aircraft Safety Icing Study." NASA/TM-2008-215107. (No. L-19435). 2008.
- [3] Lou, D. and Hammond, D.W. "Heat and Mass Transfer for Ice Particle Ingestion Inside Aero-Engine." ASME *Journal of Turbomachinery*, July 2011; 133(3): 031021. DOI 10.1115/1.4002419.
- [4] Al-Khalil, K., Horvath, C., Miller, D., Wright, W., Al-Khalil, K., Horvath, C., Miller, D., and Wright, W. "Validation of Nasa Thermal Ice Protection Computer Codes. III-The Validation of Antice." *Proceedings 35th Aerospace Sciences Meeting and Exhibit*. p. 51, 1997. Reno, Nevada (USA).
- [5] Beaugendre, H., Morency, F., and Habashi, W.G. "FENSAP-ICE's Three-Dimensional In-Flight Ice Accretion Module: ICE3D." *Journal of Aircraft* Vol. 40, No. 2 (2003): pp. 239–247.
- [6] Gutiérrez, B.A., Della Noce, A., Gallia, M., and Guardone, A. "Optimization of a Thermal Ice Protection System by Means of a Genetic Algorithm." *Proceedings International Conference on Bioinspired Methods and Their Applications*: pp. 189–200. Springer, 2020. Brussels, Belgium.
- [7] da Silva, G.A.L., de Mattos Silveiras, O., and de Jesus Zerbini, E.J.G. "Numerical Simulation of Airfoil Thermal Anti-Ice Operation, Part 1: Mathematical Modelling." *Journal of Aircraft* Vol. 44, No. 2 (2007): pp. 627–633.
- [8] da Silva G.A.L., de Mattos Silveiras, O., and Zerbini, E.J.G.J. "Numerical Simulation of Airfoil Thermal Anti-Ice Operation, Part 2: Implementation and Results." *Journal of Aircraft* Vol. 44, No. 2 (2007): pp. 634–641.
- [9] Bu, X., Lin, G., Yu, J., Yang, S., and Song, X. "Numerical Simulation of an Airfoil Electrothermal Anti Icing System." *Proceedings of the Institution of Mechanical Engineers, Part G: Journal of Aerospace Engineering* Vol. 227, No. 10 (2013): pp. 1608–1622.
- [10] Pourbagian, M. and Habashi, W.G. "Surrogate-Based Optimization of Electrothermal Wing Anti-Icing Systems." *Journal of Aircraft* Vol. 50, No. 5 (2013): pp. 1555–1563.
- [11] Pourbagian, M., Talgorn, B., Habashi, W.G., Kokkolaras, M., and Le Digabel, S. "Constrained Problem Formulations for Power Optimization of Aircraft Electro-Thermal Anti-Icing Systems." *Optimization and Engineering* Vol. 16, No. 4 (2015): pp. 663–693.
- [12] Pellissier, M., Habashi, W., and Pueyo, A. "Optimization Via FENSAP-ICE of Aircraft Hot-Air Anti-Icing Systems." *Journal of Aircraft* Vol. 48, No. 1 (2011): pp. 265–276.
- [13] Economon, T.D., Palacios, F., Copeland, S.R., Lukaczyk, T.W., and Alonso, J.J. "SU2: An Open-Source Suite for Multiphysics Simulation and Design." *Aiaa Journal* Vol. 54, No. 3 (2016): pp. 828–846.
- [14] Silva, G., Silveiras, O., Zerbini, E., Hefazi, H., Chen, H.H., and Kaups, K. "Differential Boundary Layer Analysis and Runback Water Flow Model Applied to Flow Around Airfoils with Thermal Anti-Ice." *Proceedings 1st AIAA Atmospheric and Space Environments Conference*. p. 3967, 2009. San Antonio, Texas (USA).
- [15] Bellosta, T., Parma, G., and Guardone, A. "A Robust 3D Particle Tracking Solver for In-Flight Ice Accretion using Arbitrary Precision Arithmetic." *Proceedings 8th International Conference on Computational Methods for Coupled Problems in Science and Engineering, COUPLED PROBLEMS 2019*. pp. 622–633. CIMNE, 2021. Sitges, Catalonia, Spain.

- [16] Gutiérrez, B.A., Della Noce, A., Gallia, M., Bellosta, T., and Guardone, A. “Numerical Simulation of a Thermal Ice Protection System Including State-of-the-Art Liquid Film Model.” *Journal of Computational and Applied Mathematics* Vol. 391 (2021): p. 113454.
- [17] Gori, G., Zocca, M., Garabelli, M., Guardone, A., and Quaranta, G. “Polimice: A Simulation Framework for Three Dimensional Ice Accretion.” *Applied Mathematics and Computation* Vol. 267 (2015): pp. 96–107.
- [18] Myers, T.G. and Charpin, J.P. “A Mathematical Model for Atmospheric Ice Accretion and Water Flow on a Cold Surface.” *International Journal of Heat and Mass Transfer* Vol. 47, No. 25 (2004): pp. 5483–5500.
- [19] CS-EASA, Certification Specification and Acceptable Means of Compliance for Large Airplane—Amendment 25.
- [20] CS-EASA, Certification Specification for Engine—Amendment 3.
- [21] Cavazzuti, M. “Optimization Methods: from Theory to Design Scientific and Technological Aspects in Mechanics.” Berlin, Heidelberg, Springer Berlin Heidelberg. 2012. ISBN 9783642311871. p.121-127.
- [22] Deb, K. and Agrawal, S. “Understanding Interactions Among Genetic Algorithm Parameters.” *Foundations of Genetic Algorithms* Vol. 5, No. 5 (1999): pp. 265–286.